

Large Acceptance Spectrometers for Invariant Mass Spectroscopy of Exotic Nuclei and Future Developments

T. Nakamura

2-12-1 O-Okayama, Meguro, Tokyo 152-8551, Japan

Y. Kondo

2-12-1 O-Okayama, Meguro, Tokyo 152-8551, Japan

Abstract

Large acceptance spectrometers at in-flight RI separators have played significant roles in investigating the structure of exotic nuclei. Such spectrometers are in particular useful for probing unbound states of exotic nuclei, using invariant mass spectroscopy with reactions at intermediate and high energies. We discuss here the key characteristic features of such spectrometers, by introducing the recently commissioned SAMURAI facility at the RIBF, RIKEN. We also explore the issue of cross talk in the detection of multiple neutrons, which has become crucial for exploring further unbound states and nuclei beyond the neutron drip line. Finally we discuss future perspectives for large acceptance spectrometers at the new-generation RI-beam facilities.

Keywords: RI beam, Large acceptance spectrometer, Invariant mass spectroscopy, Neutron detector

1. Invariant mass spectroscopy in RI-beam experiments

Rare isotope beams available at in-flight separators, at RIKEN (RIBF), MSU, GSI, and GANIL, have expanded physics opportunities to a wider range of $N - Z$. Accordingly, more experiments have been performed for nuclei near the drip line or even beyond [1, 2]. For such nuclei, most or all of the states are unbound (i.e., in the continuum), thereby decaying by emitting particles. The

invariant mass spectroscopy of such unbound states produced with direct reactions and fragmentation of exotic nuclei at intermediate and high energies has thus become a powerful experimental tool in RI-beam physics. Large-acceptance spectrometers play a major role, as we will show, in performing invariant mass spectroscopy experiments.

Let us take an example of the recent experiment on the $1n$ knockout reaction $^{17}\text{C}+p$ at 70 MeV/u by Satou *et al.* [3] at the RIPS facility [4] at RIKEN, where unbound states of ^{16}C were studied. In this case, decay particles ^{15}C and a neutron emitted in the forward kinematical cone were measured. From the momentum vectors of these two particles, one can reconstruct the invariant mass M_{16*} of a ^{16}C state as,

$$M_{16*} = \sqrt{(E_{15} + E_n)^2 - |\vec{P}_{15} - \vec{P}_n|^2}, \quad (1)$$

where (E_{15}, \vec{P}_{15}) and (E_n, \vec{P}_n) are the four momenta of the ^{15}C fragment and the neutron. One can extract the relative energy E_{rel} and the excitation energy E_x as,

$$E_{\text{rel}} = M_{16*} - (M_{15} + M_n), \quad (2)$$

$$E_x = E_{\text{rel}} + S_n, \quad (3)$$

where M_{15}, M_n are the masses of ^{15}C and the neutron, and S_n is the neutron separation energy (for ^{16}C , $S_n=4.25$ MeV). If the ^{15}C is produced in a bound excited state, then the γ decay energy ($E_\gamma = 740$ keV for ^{15}C) should also be measured and E_x is shifted up by E_γ , since M_{15} is replaced by $M_{15} + E_\gamma$. In the experiment, three states were found at $E_{\text{rel}}=0.46(3)$, $1.29(2)$, and 1.89 MeV that correspond to $E_x=5.45(1)$, $6.28(2)$ and 6.11 MeV. The $6.28(2)$ MeV state was found to be in coincidence with the 740 keV γ ray, and E_x is shifted accordingly.

The advantages of invariant mass spectroscopy in the study of exotic nuclei are summarized as follows.

- Good energy resolution: One can reach an energy resolution of about a few hundred keV (1σ) at $E_{\text{rel}} = 1$ MeV even for a momentum resolution of

the order of 1% [5] for the fragment and neutron individually. Note that the relative-energy resolution ΔE_{rel} follows approximately $\Delta E_{\text{rel}} \propto \sqrt{E_{\text{rel}}}$.

- Kinematic focusing: Since the outgoing particles are boosted by the beam velocity at intermediate and high energies, they are emitted in a narrow kinematical cone. Consequently, one can detect the decay particles with high geometrical efficiency.
- Thick target: Since one uses intermediate and high energy beams, one can use a comparatively thick target of the order of 100 mg/cm² at 50-70 MeV/u to 1 g/cm² at 200 MeV/u. Hence, one can obtain high reaction yield, which is important for RI-beam experiments since beam intensity is generally weak.

Owing to these advantages invariant mass spectroscopy has become one of the most useful methods to study the continuum structure of exotic nuclei. There is, however, one disadvantage: One needs to measure all the outgoing beam-velocity particles, which makes the experiment and the analysis more complicated. For instance, if the daughter nucleus is in a high-lying excited state, then this may decay by a cascade of γ rays. In this case, an accurate measurement of the excitation energy requires a high-efficiency γ -ray calorimeter.

To realize invariant mass spectroscopy, a large acceptance spectrometer is highly desirable. In the above example [3], a simple dipole magnet was used in combination with the neutron-detector array based on plastic scintillators (see Fig. 1 of Ref. [6], the “RIPS-Dipole setup”), which was a pioneering invariant-mass-spectroscopy setup at the RIPS facility at RIKEN since 1992. This dipole magnet has a relatively large gap (30 cm), so that the outgoing particles including neutrons have a large acceptance. On the other hand, the momentum resolution is moderate (1%) since focusing elements such as quadrupole magnets are not used. A momentum resolution of 1% is already sufficient to obtain a good E_{rel} resolution, and a simple dipole magnet has an advantage of having large acceptance. The use of such a magnet is also necessary to “sweep” the charged particles away from the neutron detectors.

A large momentum acceptance of the magnet is advantageous in studying a variety of final states with a single setup. Let us consider the incident beam of the drip-line nucleus ^{22}C on a carbon target. In this case, one can study its reaction cross section of ^{22}C to study its size, $1n$ removal to study the unbound ^{21}C states ($\rightarrow ^{20}\text{C}+n$), low-lying excited states ^{22}C with the inelastic scattering, and other unbound states such as $^{16,17,18,19}\text{B}$ with proton-removal fragmentation reactions, for example.

2. SAMURAI Facility at RIBF

At the RIBF, RIKEN, the advanced invariant-mass-spectrometer setup, SAMURAI was constructed and commissioned in 2012 [7, 8, 9]. SAMURAI stands for **S**uperconducting **A**nalysers for **M**ulti particles from **R**adio **I**sotope **B**eams. The SAMURAI setup for the invariant mass spectroscopy of neutron-rich nuclei is schematically shown in Fig. 1(a). This setup was used, as shown, for the recent kinematically complete measurement of the unbound system ^{26}O by $1p$ knockout from ^{27}F with a carbon target at 201 MeV/u [10].

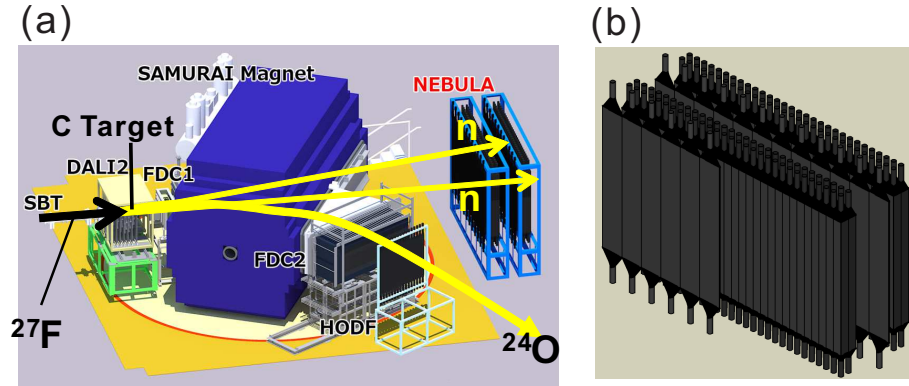


Figure 1: (a) The SAMURAI setup for the invariant mass spectroscopy of neutron-rich nuclei, as used for the study of the unbound states of ^{26}O [10]. (b) The NEBULA neutron detector array. The first veto layer is partially removed for display purposes.

The principal element is the superconducting SAMURAI magnet with a

maximum field of 3.1 Tesla (Field integral 7.1 Tm) with a large effective gap of 80 cm. One characteristic feature of the SAMURAI facility is its relatively high momentum resolution for the charged fragment, of the order of 10^3 (1σ). This was realized by designing the magnet to have a large bending angle of about 60 degrees, as well as the tracking using four multi-wire drift chambers with high position resolutions [7]. A simple tracking analysis using a polynomial fit and the calculated field map, combined with a time-of-flight measurement between the target and the hodoscope (HODF), can already provide $P/\Delta P \sim 700$ (σ), the design value of SAMURAI. With detailed tracking and restricted acceptance, the momentum resolution can reach about 1500 [7]. The interest of high-momentum resolution is that it provides for high mass resolution in the particle-identification. When one needs sufficient separation in the mass distribution $\sim 5\sigma$ separation may be necessary when a particular isotope has a much larger yield compared to the neighbors. Such a high separation (5σ) is indeed achieved for charged fragments with $A \sim 100$ when the momentum resolution is $P/\Delta P = 700$. Figure 2 (left) shows the particle identification spectrum obtained in the ^{26}O experiment. The mass spectrum extracted for the oxygen isotopes is shown in Fig. 2 (right), where better than $\sim 10\sigma$ separation is reached in this mass region. Recently, an experiment on ^{132}Sn was performed where masses are clearly separated even in this mass region [11].

Neutrons emitted in the forward direction go through the gap of the magnet and their positions and time-of-flight are measured by the neutron detector array NEBULA (**N**eutron-detection system for **B**reakup of **U**nstable-Nuclei with **L**arge **A**cceptance), which is shown schematically in Fig. 1(b). The NEBULA array consists of 120 modules of plastic scintillator, each of which is $12(\text{W}) \times 12(\text{D}) \times 180(\text{H}) \text{ cm}^3$. These modules are arranged into two walls, each of which is composed of two layers of 30 modules. The total thickness is thus 48 cm [7], and the area amounts to $360 \times 180 \text{ cm}^2$. In the ^{26}O experiment, the front faces of these two walls were 11.12 m and 11.96 m downstream of the reaction target. Each wall is equipped with a charged-particle veto array of 1 cm thickness. A wide acceptance is required since neutrons are emitted with much

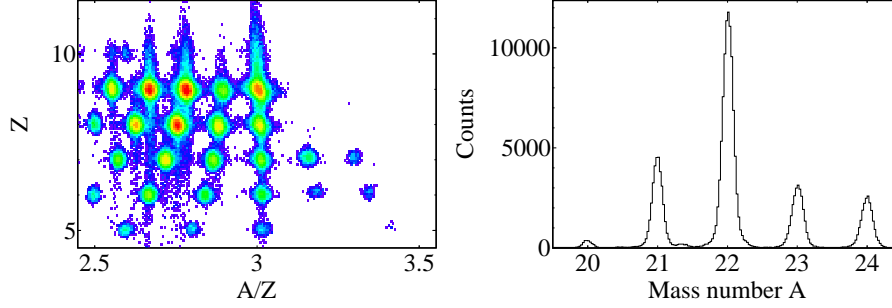


Figure 2: Left: particle identification spectrum of the charged fragments for $^{27}\text{F}+\text{C}$ at 201 MeV/u, obtained from the tracking and the TOF between the target and the hodoscope (HODF). Right: The mass spectrum of the oxygen isotopes.

larger angles than the charged fragment, as discussed below.

The other important feature of SAMURAI as an advanced large-acceptance facility is that it offers a variety of experimental modes, which are owing to the rotatable stage on which the magnet is installed. The range of rotation is -5° to 95° degrees (0° corresponds to the setup where the entrance and exit faces are 90° to the beam axis). The setup in Fig. 1(a) is at 30° . SAMURAI thus offers a variety of experimental setups, e.g., for 1) Invariant mass spectroscopy by HI(Heavy-ion fragment) + neutron(s) coincidences as in the example of ^{26}O , 2) Invariant mass spectroscopy by HI+proton coincidence at the 90° setting, where the hole in the yoke is used as a beam port, 3) Missing mass spectroscopy by measuring recoil particles primarily from the target, 4) Polarized deuteron-induced reactions, and 5) Heavy-ion collisions to measure π^\pm using the TPC(Time Projection Chamber) [12] in the gap of the magnet at the 0° setting. As such, SAMURAI is a unique facility capable of supporting a very versatile nuclear physics program.

3. Large-acceptance spectrometers vs. High-resolution spectrometers

As with the SAMURAI facility, large-acceptance spectrometers have been constructed at many in-flight RI-beam facilities, and played significant roles in the spectroscopy of unstable nuclei. At RIKEN, as mentioned, before SAMURAI was commissioned, a smaller RIPS-Dipole setup had been used. At the NSCL at MSU, the Sweeper superconducting magnet is installed [13], combined with the large acceptance neutron array MoNA and LISA [14]. At GSI, the ALADIN/LAND setup has long been used, and it is now being upgraded to the R³B setup for the FAIR facility [15].

The characteristic features of the large-acceptance spectrometers are now discussed, in comparison with the high-resolution spectrometers. Table 1 compares the characteristic features. The momentum resolution ($P/\Delta P$) is of the order of $10^2 - 10^3$ for the large acceptance spectrometers, while that is the order of 10^4 for the high resolution spectrometers. The large acceptance spectrometer is intended primarily for invariant mass spectroscopy, while the high resolution spectrometer is for missing mass spectroscopy which requires higher momentum resolution.

It is worth noting that high acceptance is needed for the invariant mass spectroscopy for exotic nuclei for the sake of the neutron (proton) detection. For instance, let us consider the invariant mass spectroscopy of AZ breaking up into ${}^{A-1}Z + n$. In this case, it is easily shown that the emission angle for neutron, θ_n , is roughly $A - 1$ times the angle θ_f for the charged fragment, due to the momentum balance in the center-of-mass frame. Hence, the acceptance is more crucial for neutron detection. The opening angle θ between the neutron and the fragment is then close to θ_n . The relative energy is approximately

$$E_{\text{rel}} = \frac{1}{2}\mu v_{\text{rel}}^2 \sim \frac{E}{A}\theta_n^2, \quad (4)$$

where E is the incident beam energy. This simple consideration demonstrates that when the neutron detectors and the gap of the magnet allow a measurement

Table 1: Comparison of large-acceptance and high-resolution spectrometers. RIPS-Dipole setup and SAMURAI represent the large acceptance spectrometers, while SHARQA and the S800 Spectrograph represent the high resolution spectrometers. The angular acceptance for the large-acceptance spectrometer is for neutrons, while that for the high-resolution spectrometer is for the charged particle residue (ejectile).

	RIPS-Dipole	SAMURAI [7]	SHARQA [16]	S800 [17]
$P/\Delta P$	~ 100	~ 1000	15000	10000
Angular Ac- ceptance	~ 100 mstr	~ 50 mstr	4.8 mstr	20 mstr
Momentum Acceptance	~ 50 %	~ 50 %	2%	$\sim 5\%$
$B\rho_{\text{MAX}}$	~ 4.2 Tm	~ 7 Tm	6.8 Tm	4 Tm
Configuration	D	D	QQDQD	QQDD

of the neutrons up to $\theta_n = 5^\circ(10^\circ)$, then events of $E_{\text{rel}} \simeq 2$ (8) MeV are fully accepted.

4. Neutron detection and cross talk rejection at SAMURAI/NEBULA

The NEBULA array is, as with the other high-energy neutron detector arrays such as MoNA [14] and NeuLAND [15], based on plastic scintillator. The performance of the NEBULA array was investigated, using the simulation code GEANT4 with the QGSP_INCLXX physics model (intranuclear cascade model) for the neutron interactions in NEBULA. The simulation was then compared with the experimental results using the ${}^7\text{Li}(p, n){}^7\text{Be}$ reaction at 200 MeV where the ground and the 1st excited states of ${}^7\text{Be}$ were populated. This reaction can thus deliver nearly mono-energetic neutrons, and thus has long been used for the evaluation of the characteristics of neutron detectors. From the simulation, we found that the intranuclear cascade model used here reproduces the experimental results rather well as shown below at energies around 200 MeV. We note that neutron detection below 100 MeV is well understood with MENATE_R [18, 19],

an updated version of MENATE [20].

In the invariant mass spectroscopy of neutron-rich nuclei, coincidence detection of more than one neutron becomes more important. For instance, in the Coulomb breakup of two-neutron halo nuclei, such as ^{11}Li , one needs to measure $^9\text{Li}+n+n$ [6]. In the study of ^{26}O , one needed to measure $^{24}\text{O}+n+n$. In the near future, the challenge of detecting four neutrons in coincidence will need to be confronted for the study of ^{28}O . In such cases, one needs to eliminate so-called “cross talk”, where one neutron can produce more than one signal that may mimic multi-neutron events. Such cross-talk events can be investigated using the $^7\text{Li}(p,n)^7\text{Be}(\text{g.s.}+0.43\text{MeV})$ reaction that emits only a single neutron. As such, all the multiplicity-greater-than-one events in the NEBULA array are judged as cross-talk events.

Here, we consider primarily how to treat the two-neutron coincidence events to distinguish them from the cross talk. There are two ways to detecting two neutrons in an array such as NEBULA: i) Different-wall events: one neutron detected in the 1st wall and the other neutron in the 2nd wall, ii) Same-wall events: both of the neutrons are detected in the same wall, either in the 1st or 2nd wall. We discuss these two cases separately. We note that cross-talk rejection procedures have also been developed at lower energies [21, 22].

4.1. Cross talk in different-wall events

The cross talks relevant to the different-wall events are schematically illustrated in Fig. 3. The spectra of the cross talk events (multiplicity $M \geq 2$ in the NEBULA modules) induced by single quasi-monoenergetic neutrons in the $^7\text{Li}(p,n)^7\text{Be}$ reaction at 200 MeV is shown in Fig. 4. The energy threshold of the detectors was set to be 6 MeVee (electron equivalent) to remove most of the γ rays produced in the scintillator.

The left spectrum is shown as a function of the charge Q_1 obtained in a module in the 1st wall versus the velocity ratio β_{01}/β_{12} (left), while the right figure is shown as a function of the pulse height Q_2 obtained in a module in the 2nd wall versus $1/\beta_{12}$ (right). Here β_{01} represents the velocity between the

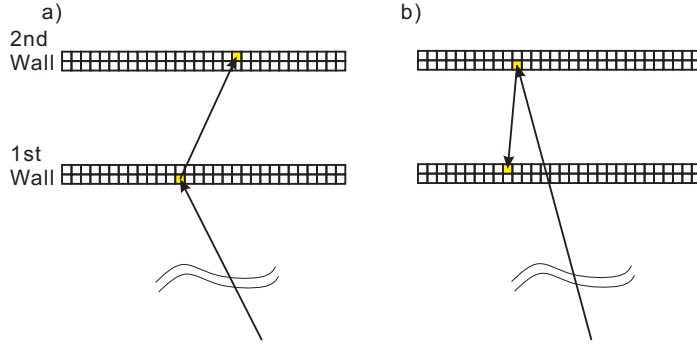


Figure 3: Examples of cross-talk events relevant to the different wall events. (a) A single neutron is scattered and leaves a signal in a module in the 1st Wall, then leaves another signal in a module in the 2nd Wall. (b) A single neutron is registered in a scintillator in the 2nd wall, and the evaporated neutron is detected in the 1st Wall.

target and the first registered module, while β_{12} is that between the first and the second registered modules. If the first signal is registered in the 2nd wall, β_{12} is negative.

The main cross-talk component, which lies to the right of the line in Fig. 4 (left), is due mainly to the quasi-free scattering on ^{12}C , and to the scattering of the neutron by a proton (hydrogen) in the scintillator material. This corresponds to the event shown in Fig. 3(a). In this case, the neutron after the 1st wall is slower than the neutron before the 1st wall, and thus $\beta_{01}/\beta_{12} > 1$. The line in Fig. 4(left) represents the boundary of this component, and is tilted since the more the energy that is lost in the first wall, the smaller the β_{12} (and the larger the β_{01}/β_{12}). In the rejection procedure in an experiment involving two neutrons, the events on the right hand side of this line are eliminated.

On the other hand, there are much fewer events with $\beta_{01}/\beta_{12} < -1$, which are interpreted as neutrons arising from neutrons evaporated from the 2nd wall. This component corresponds to the event shown in Fig. 3(b). Such neutrons are expected, as observed in Ref. [23], from the interaction of high energy nucleons with the C nuclei.

Figure 4(right) shows the spectrum of Q_1 vs. $1/\beta_{12}$, which shows more

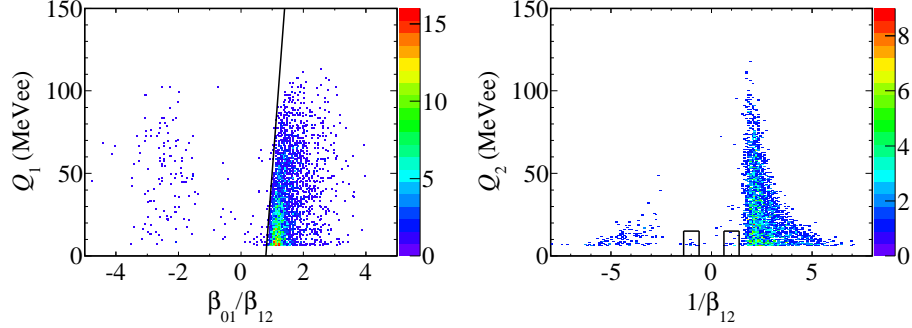


Figure 4: Spectra of the multiplicity $M \geq 2$ events observed in the ${}^7\text{Li}(p, n){}^7\text{Be}$ reaction. Left: Q_1 (pulse height in the 1st wall) versus β_{01}/β_{12} . The right hand side of the line is caused by the event shown in Fig. 3(a), while the events $-4 < \beta_{01}/\beta_{12} < -1$ correspond to Fig. 3(b). Right: Q_2 (pulse height in the 2nd wall) versus $1/\beta_{12}$. The squares represent for the cut for the γ -ray cross talk.

clearly the events arising from γ rays that traverse the two walls. The squares shown in the figure are the conditions used to eliminate the γ -ray cross talk. It should be noted that these γ -ray cross talk events are produced in the detector material, and not caused by the reaction at the target.

The projection onto the velocity ratio in the ${}^7\text{Li}(p, n){}^7\text{Be}$ reaction is shown in Fig. 5, compared with the GEANT4 simulation. As shown, the cross-talk events are well reproduced by the simulation.

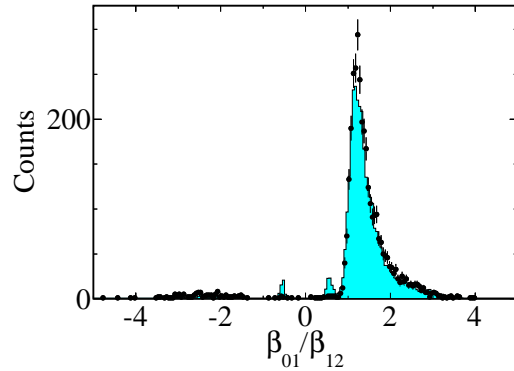


Figure 5: β_{01}/β_{12} distribution (solid points) obtained in the ${}^7\text{Li}(p, n){}^7\text{Be(g.s.}+0.43\text{ MeV)}$ reaction, which is compared with the GEANT4 simulation (histogram). The small peaks at $\pm \sim 0.6$ are due to γ rays ($\beta_{12} = 1, \beta_{01} = 0.57$).

4.2. Cross talk in same-wall events

The cross talk relevant to same wall events are schematically shown in Fig. 6. In this case, the cross talk occurs mostly between neighboring modules.

Figure 7 shows spectra of the time difference (dt) against the distance (dr) between the two hits in the same wall in the ${}^7\text{Li}(p,n){}^7\text{Be}$ data (left). Here, $dt = t_2 - t_1$ and $dr = |\vec{r}_2 - \vec{r}_1|$, where (t_1, \vec{r}_1) , and (t_2, \vec{r}_2) are respectively the timing and three-dimensional coordinate of the two signals in the same wall caused by a single neutron. As shown the results of the simulation are almost identical to the experimental data. The agreement between the data and the simulation is even more clearly seen in the projected dr and dt distributions shown in Fig. 8, demonstrating the validity of the simulation.

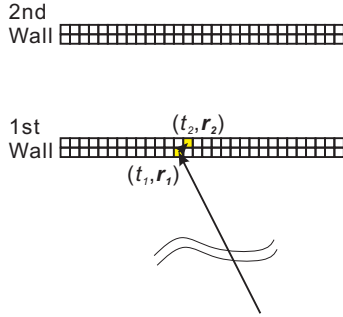


Figure 6: Examples of cross-talk events relevant to same wall events.

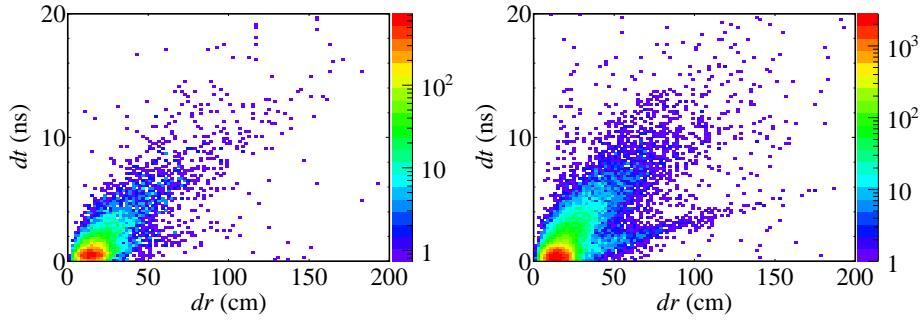


Figure 7: Plots of the two hit events (both in the 1st wall, or both in the 2nd wall) observed in the ${}^7\text{Li}(p,n){}^7\text{Be}$ reaction. Left: Experimental spectrum of dr versus dt . Right: Results of the simulation.

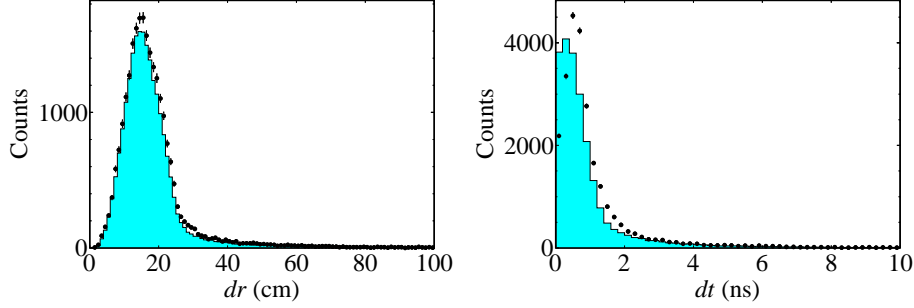


Figure 8: Solid dots are experimental data of the distance (left) and the time difference between the two hits in the ${}^7\text{Li}(p,n){}^7\text{Be}(\text{g.s.}+0.43\text{ MeV})$ reaction, relevant to the cross-talks in the same wall. Results from the simulation are shown by the solid histograms.

The cross-talk events are rejected using the condition,

$$\sqrt{\left(\frac{dr - dr_0}{R}\right)^2 + \left(\frac{dt - dt_0}{T}\right)^2} < 1, \quad (5)$$

where $dr_0 = 15.8\text{ cm}$, $R = 15.0\text{ cm}$, $dt_0 = 0.50\text{ ns}$, and $T = 18.3\text{ ns}$ were determined empirically. In this case, the first hit is adopted as a representative hit.

4.3. Evaluation of cross-talk cuts

Figure 9 shows the multiplicity distribution of the single neutron from the ${}^7\text{Li}(p,n){}^7\text{Be}$ reaction and the simulation, before (a) and after (b) the cross talk elimination procedure. Firstly, as shown, the experimental results are well reproduced by the simulation both before and after the cross talk elimination. Secondly, the vast majority of the cross talk is eliminated: most of the events with $M \geq 2$ are either eliminated or summed up to the $M = 1$ events. More specifically, 97.1% of the cross talk is eliminated in the ${}^7\text{Li}(p,n){}^7\text{Be}$ data, while 98.4% is eliminated in the simulation. This further demonstrates that the cross talk is well understood and the rejection procedures are valid.

Finally, the efficiency for the two neutron detections are estimated as shown in Fig. 10. The very low E_{rel} less than 200 keV are unsurprisingly more efficiently

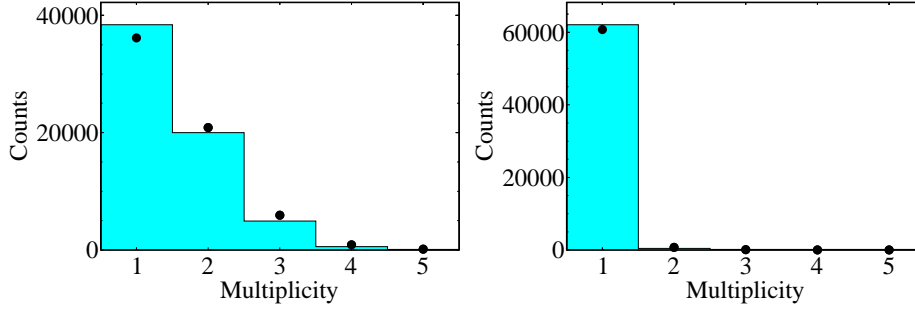


Figure 9: Multiplicity distribution obtained for the ${}^7\text{Li}(p, n){}^7\text{Be}$ reaction before the cross-talk rejection (left) and after (right). The solid dots are experimental results, while the histograms are obtained from the simulation.

detected in different walls as the neutrons are emitted with a small opening angle. On the contrary, the $2n$ efficiency drops rapidly for the same wall events below 200 keV due to the cross-talk rejection procedure (Eq. 5).

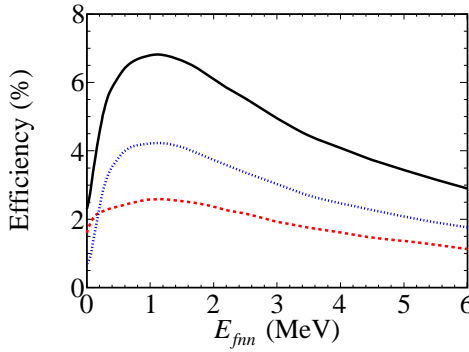


Figure 10: Two-neutron detection efficiency obtained by the simulation for the case of ${}^{26}\text{O} \rightarrow {}^{24}\text{O} + n + n$ produced by $1p$ removal from ${}^{27}\text{F}$ at 201 MeV/u. The different-wall events are shown by the red dashed line, while the same-wall events are the blue dotted line. The sum is shown by the black solid line.

5. Summary and Future prospects

We have shown that large-acceptance spectrometers are a very useful tool for probing nuclei at the limits of stability. Some key elements are: 1) large

acceptance for neutron detection, and 2) relatively high resolution for clear mass identification. These features have been realized, as shown here, in the advanced large-acceptance spectrometer SAMURAI. We have also discussed the issue of cross-talk when we need to measure multiple neutrons. In particular, we have shown that a multi-wall neutron detector array is well suited to such studies and provides good detection efficiencies even at low E_{rel} .

In the near future, at SAMURAI, it is planned to measure the $4n$ decay of ^{28}O . To realize such an experiment, the MINOS target [24] and the NeuLAND neutron detectors have been added to the setup. MINOS is a thick cryogenic LH_2 (liquid hydrogen) target coupled to a light-particle tracker for the vertex reconstruction. Hydrogen has the most atoms per gram, which is significant to maximize the yield of ^{28}O . Since MINOS can determine the vertex, the ambiguity of the energy loss in the target is reduced. Hence, relatively good energy resolution is expected even with such a thick target (~ 15 cm).

Neutron detectors with large volume and high granularity is also important to measure more than two neutrons. Due to the cross talk rejection procedures, the larger the number of separated walls the better the neutron detection efficiency. With such a motivation, 400 NeuLAND modules ($5 \times 5 \times 250$ cm³ each) have been installed at SAMURAI, in addition to the existing NEBULA detectors, for the next 2-3 years. An upgrade of the NEBULA array, NEBULA-Plus proposed by the LPC group (Orr *et al.*), has been approved, which will also facilitate multi-neutron measurements.

In FRIB at MSU, the HRS (**H**igh **R**igidity **S**pectrometer) project has been proposed [25, 26]. As discussed here, one of the important requirements of an advanced large acceptance spectrometer is a high momentum resolution for charged fragments, in particular to separate heavier masses. The HRS will be equipped with focusing elements (quadrupoles) which can provide for the high momentum resolution. A sweeper magnet with a large gap will also be developed, to provide for a large acceptance for neutrons ($\pm 6^\circ$), when MoNA and LISA are used in the forward direction.

For the future FAIR facility, the development of R^3B (Reactions with Rela-

tivistic Radioactive Beams) is underway. This includes the large superconducting dipole magnet (field integral $BL \sim 5$ Tm), and 3000 NeuLAND modules to realize a $4n$ detection efficiency of nearly 60% [15]. As mentioned, some of the first NeuLAND modules have been introduced to RIBF, in advance of the experiments at FAIR. Early physics runs with the R^3B setup at GSI are also expected in 2018.

Advanced large acceptance spectrometers are being built and developed world-wide. Many more opportunities for physics studies are expected, as new associated devices are added. As such, we expect that the large acceptance spectrometers will continue to play significant roles in the next decade in RI-beam physics.

Acknowledgment

The authors would like to thank the SAMURAI collaboration. In particular, H. Otsu, T. Kobayashi, N.A. Orr, J. Gibelin, M. Marques, Y. Satou, M. Sasano, J. Yasuda, T. Isobe, T. Murakami, T. Motobayashi, V. Panin, Y. Togano, S. Koyama, R. Tanaka, J. Tsubota, M. Shikata, T. Ozaki, A. Saito, K. Yoneda, H. Sato, T. Kubo, and T. Uesaka. We are grateful to M. Thoennessen and T. Aumann for giving T.N. slides and materials.

References

- [1] I. Tanihata, H. Savajols, R. Kanungo, Prog. Part. Nucl. Phys. 68 (2013) 215.
- [2] T. Baumann, A. Spyrou, M. Thoennessen, Rep. Prog. Phys. 75 (2012) 036301.
- [3] Y. Satou, et al., Phys. Lett. B 728 (2014) 462.
- [4] T. Kubo, et al., Nucl. Instr. and Meth. B 70 (1992) 309.
- [5] T. Aumann, T. Nakamura, Phys. Scr. T152 (2013) 014012.

- [6] T. Nakamura, et al., Phys. Rev. Lett. 96 (2006) 252502.
- [7] T. Kobayashi, et al., Nucl. Instr. and Meth. B 317 (2013) 294.
- [8] H. Shimizu, et al., Nucl. Instr. and Meth. B 317 (2013) 739.
- [9] H. Sato, et al., IEEE Trans. Appl. Supercond. 17 (2013) 4500308.
- [10] Y. Kondo, et al., Submitted to Phys. Rev. Lett. (2015).
- [11] J. Yasuda, et al., Submitted to Nucl. Instr. and Meth. B (EMIS15 proceedings) (2015).
- [12] R. Shane, et al., Nucl. Instr. and Meth. A 784 (2015) 513.
- [13] M. Bird, et al., IEEE Trans. Appl. Supercond. 15 (2005) 1252.
- [14] T. Baumann, et al., Nucl. Instr. and Meth. A 543 (2005) 517.
- [15] T. Aumann, the R³B collaboration, R³B technical design report, 2011.
http://www.fair-center.eu/fileadmin/fair/publications_exp/NeuLAND-TDR-Web.pdf.
- [16] T. Uesaka, S. Shimoura, H. Sakai, Prog. Theor. Exp. Phys. 2012 (2012) 03C007.
- [17] D. Bazin, et al., Nucl. Instr. and Meth. B 204 (2003) 629.
- [18] B. Roeder, "development and validation of neutron detection simulations for eurusol", eurusol design study, report, 2008.
http://www.eurusol.org/site02/physics_and_instrumentation/S.
- [19] Z. Kohley, et al., Nucl. Instr. and Meth. A 682 (2012) 59.
- [20] P. Desquelles, Nucl. Instr. and Meth. A 307 (1991) 366.
- [21] J. Wang, et al., Nucl. Instr. and Meth. A 397 (1997) 380.
- [22] F. Marques, et al., Nucl. Instr. and Meth. A 450 (2000) 109.
- [23] Y. Iwamoto, et al., J. KPS 59 (2011) 1753.

- [24] A. Obertelli, T. Uesaka, Eur. Phys. J. A 47 (2011) 105.
- [25] T. Baumann, et al., Submitted to Nucl. Instr. and Meth. B (EMIS15 proceedings) (2015).
- [26] A. Gade, R. Zegers, editors, HRS - a high rigidity spectrometer for FRIB, 2014. <http://hrs.lbl.gov/home>.